MRS Advances

Comparison of neutral and charged polyelectrolyte bottlebrush polymers in dilute salt-free conditions

Alexandros Chremos[1] and Ferenc Horkay[1]

[1]Section on Quantitative Imaging and Tissue Sciences, *Eunice Kennedy Shriver National Institute of Child Health and Human Development,* National Institutes of Health, Bethesda, MD 20892, USA

Abstract: We investigate the structure of neutral and charged bottlebrush polymers in salt-free solutions at different polymer concentrations. In particular, we use molecular dynamics simulations by utilizing a coarse-grained bead-spring model that includes an explicit solvent and complementary experiments made by small angle neutron scattering (SANS). We find that the charged groups along the side chains exert significant repulsive forces, resulting in polymer swelling and backbone stretching. In addition to the primary polyelectrolyte peak, we find that bottlebrush polymers exhibit an additional peak in the form and static structure factors, a feature that is absent in neutral polymers. We show that this additional peak describes the intra-molecular correlations between the charged side chains.

INTRODUCTION

Bottlebrush polymers are highly branched macromolecules composed of tightly spaced side chains tethered along a polymer backbone chain. The packing of side chains results in strong excluded volume effects, leading to extended conformations that typically precludes the development of intermolecular entanglements and results in materials with Rouse-like relaxation dynamics, i.e., no rubbery plateau [1]. This type of polymers have gained considerable interest in recent years because of their wide range of applications, including rheological modifiers, nanoporous materials, supersoft elastomers, and photonic bandgap materials [1-6]. Moreover, bottlebrush polymers play an important role in certain biological systems. For example, the main cartilage proteoglycan aggrecan exhibits a bottlebrush structure and is important in the proper functioning of articular cartilage. It forms large microgel-like complexes (via its interaction with hyaluronan and link protein) that endows cartilage with load-bearing properties [7-10]. Degradation of aggrecan due to aging, injury, or diseases can lead to loss of mechanical properties and severe chronic pain. However, the design and creation of synthetic aggrecan remains a challenge because it is poorly understood how the molecular characteristics of the bottlebrush architecture contribute to the macroscopic properties and function of cartilage.

The challenge in modeling bottlebrush polymers is that their molecular architecture has multiple molecular parameters, such as grafting density, side chain length, and backbone length, which influence the polymer conformations in non-trivial ways. In the case of aggrecan, a more complicated picture emerges because the side chains carry charged groups that release counter-ions in polar solvents, thus turning the polymer into a polyelectrolyte. Even in linear chain polyelectrolytes, the long-range Coulomb interactions can result in a complex coupling between the diffuse ionic cloud of dissolved counter-ions and the polyelectrolyte molecules [11-18]. In polyelectrolyte bottlebrushes both the complexity of the molecular architecture and the coupling of long-range Coulomb interactions further increase the challenge of predicting the bottlebrush conformations and gel structure.

In the absence of a predictive fundamental theory, we investigate neutral and polyelectrolyte bottlebrush polymers in salt-free solution in the dilute regime with molecular dynamics simulations using a bead-spring polymer model having explicit solvent. We calculate the radius of gyration and hydrodynamic radius. Based on these quantities we determine the average molecular size and discuss the role of charged groups along the polymer structure. For these model polymers, we also probe the structure by calculating the form and static structure factors as well as inter-molecular pair correlations. Our findings are discussed in light of small angle neutron scattering (SANS) experiments towards identifying the key factors that influence the physical behavior of bottlebrush polymers.

METHODOLOGY

Computer simulations

We employ molecular dynamics simulations based on a bead-spring polymer model with stiff harmonic bonds suspended in an explicit solvent. The system is composed of a total of $N = 252\,000$ interaction centers in a periodic cube of side L. There are $N_p = 5, 10, 20,$ and 40 bottlebrush polymers, having a backbone chain length of $N_b = 40$ segments, $f = 40$ side chains distributed uniformly along the backbone chain, and each side chain is composed of 12 polymer segments, see schematic of the polymer model in Fig. 1a. For comparison reasons, we also briefly examine the case of bottlebrushes having $f = 10$ side chains. Thus, the polymer has a molecular mass $M_w = f M + N_b = 520$. Polyelectrolyte bottlebrush polymers carry a total charge $-Z_p e = -f M e$ distributed uniformly along the side chains, where e is the elementary unit of charge; the backbone of polyelectrolyte bottlebrushes does not carry charges. The system is electro-neutral, thus there are $N_+ = f M$ counter-ions. The number of solvent particles is $N_s = N - N_p M_w - N_+$. In the case of charged polymers, some of the solvent particles are charged to represent counter-ions.

All polymer (both neutral and charged) segments, dissolved ions, and solvent particles are interacting with the Lennard-Jones (LJ) potential and they are assigned the same mass m, diameter σ, strength of interaction ε. We set ε and σ as the units of energy and length and the cutoff distance for LJ interaction potential is $r_c = 2.5\,\sigma$. All interaction parameters are set equal to unity, unless stated otherwise. The choice of the parameters between the solvent and the polymer corresponds to good solvent condition with a Flory-Huggins parameter $\chi = 0$ [19]. In our model, the counter-ion represents sodium (Na$^+$); this is done by setting the dispersion energy interaction between the solvent particles and

the counterions, $\varepsilon_{cp} / \varepsilon = 1.25$ [20,21]. All charged particles interact via the Coulomb potential and the particle-particle particle-mesh method is used. In the simulations that include polyelectrolyte bottlebrushes, the strength of the Coulomb interactions is specified by the Bjerrum length $l_B / \sigma = e^2 / \epsilon_r kT = 1.85$, where ϵ_r is the dielectric constant of the medium.

The operating conditions are typical of the LJ liquid state: reduced temperature $kT / \varepsilon = 0.75$, the latter is maintained by a Nosé-Hoover thermostat. Typical simulations equilibrate for 4 000 τ and data is accumulated over a 10 000 τ interval, where $\tau = \sigma (m / \varepsilon)^{1/2}$ is the unit of time. The box size was $L = 70 \sigma$.
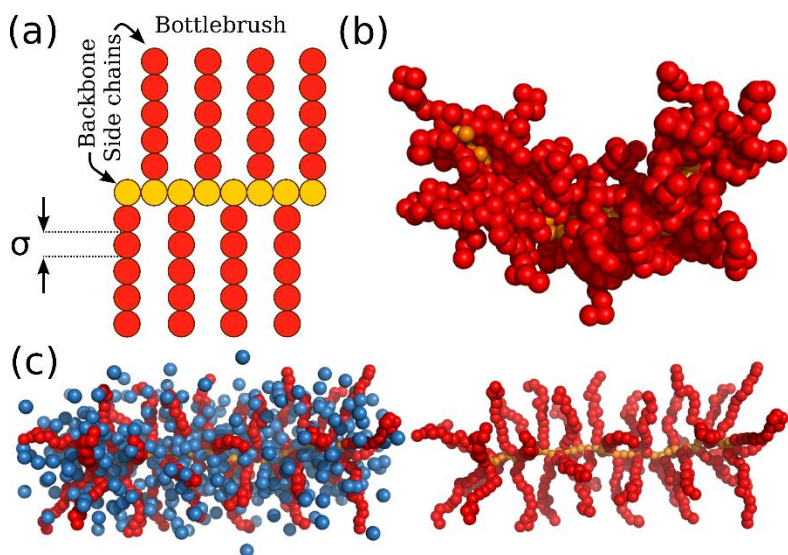
Figure 1: (a) Schematic of the bottlebrush molecular architecture. (b) Typical molecular configuration of a neutral bottlebrush polymer in dilute solution; the side chains are rendered transparent for clarity. (c) Typical molecular configuration of a charged bottlebrush polymer in dilute solution, having the nearby counter-ions visible (left) and invisible (right) for visualization purposes.

Small-Angle Neutron-Scattering Measurements

SANS measurements were made on the 10 m Small Angle Neutron Scattering instrument at National Institute of Standards and Technology (NIST) on a sample of poly(tert-butyl acrylate) (PtBA) bottlebrush solution, using a wavelength of $\lambda = 8$ Å, with wavelength spread $\Delta\lambda / \lambda = 0.13$. Two sample-detector distances were used, 4 m and 10 m, corresponding to an explored wave vector range 0.003 Å^{-1} $< q <$ 0.2 Å^{-1} where $q = (4\pi/\lambda) \sin(\theta/2)$, with θ being the scattering angle. The sample temperature during the experiment was maintained at 25 $\pm$ 0.1 $^\circ$C. After radial averaging, corrections for incoherent background, detector response and cell window scattering were applied. The neutron-scattering intensities were calibrated using water [22].

DISCUSSION

We start the discussion with the characterization of neutral and charged bottlebrush polymers in dilute solutions. We calculate the average radius of gyration $<R_g>$ and hydrodynamic radius $<R_h>$ at different polymer concentrations in the dilute regime. It is evident from the results presented in Fig. 2 that charged bottlebrush polymers are larger in size both in $<R_g>$ and $<R_h>$. As seen from screenshots of typical molecular configurations in Fig. 1, the size of the polymer is increased primarily due to the effective repulsive interactions between the side chains resulting in the stretching of the backbone of the bottlebrush polymer and the side chains perpendicular to backbone. The size of neutral polymers in the dilute regime is not significantly influenced by the polymer concentration, c. It has been argued that the size of the bottlebrush polymers progressively shrinks as c approaches the overlap concentration, c^* [23]. On the other hand, the size of the charged bottlebrush polymer is influenced by c due to screening of electrostatic interactions by the higher charge density, i.e., charged polymer segments and counter-ions, in the system at higher values of c. We note that in Fig. 2c is normalized by the overlap concentration defined as $c^* = 1/[R_g(c \rightarrow 0)]^3$, where $R_g(c \rightarrow 0)$ is determined by extrapolation from the three lowest polymer concentrations. Thus, when we compare neutral and charged bottlebrush polymers in solution at the same range of polymer concentrations, the resulting values of c^* are different. The progressive decrease of the bottlebrush polyelectrolyte size with c occurs at $c/c^* \approx 0.1$, while the same effect occurs at $c/c^* > 0.4$ for the neutral bottlebrush polymer in solution (not shown here). This effect signifies that bottlebrush polyelectrolytes are more sensitive than the corresponding neutral polymers to changes in their conditions, making them ideal for stimuli-responsive material.
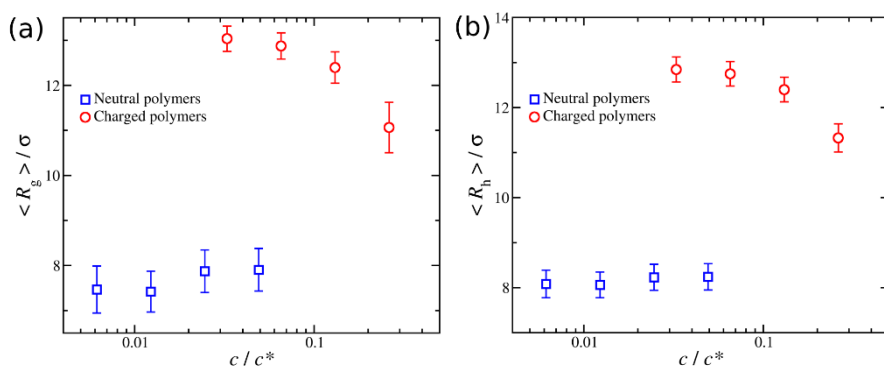
Figure 2: (a) Average radius of gyration $< R_g >$ and (b) average hydrodynamic radius $< R_h >$ of neutral and charged bottlebrush polymers at different polymer concentrations, c, normalized by the overlap concentration, $c^* = 1 / [R_g(c \rightarrow 0)]^3$. Error bars represent two standard deviations.

Now that we have a basic understanding of the relevant polymer sizes, it is equally important to quantify the shape of these polymers. We calculate the ratio $<R_h> / <R_g>$ which is often used to describe the average molecular shape of polymers; the calculation of R_h is based on the friction coefficient of an arbitrary shaped Brownian particle. The values of R_h / R_g for a smooth sphere is 1.29, for a random walk is 0.79, and for an infinite long rod is 0 [24,25]. Interestingly, $<R_h> / <R_g>$ is approximately the same for neutral and charged bottlebrush polymers, indicating that electrostatic interactions

increase the dimensions of the polymer in every direction proportionally, so that the average molecular shape remains unchanged, see Fig. 3.
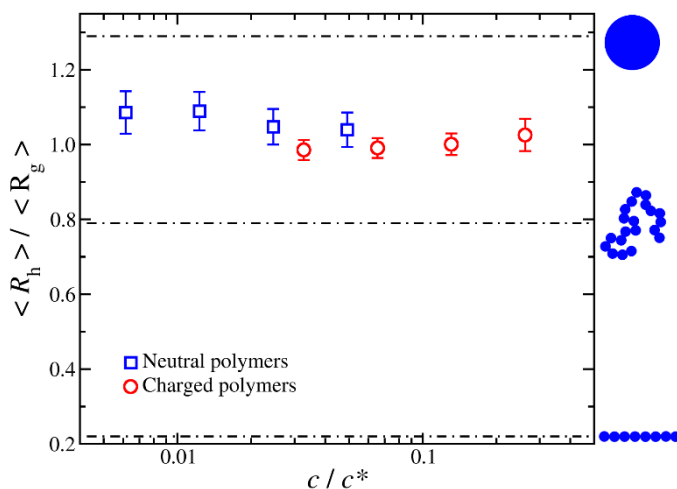
Figure 3: Ratio of average hydrodynamic radius over the radius of gyration, $<R_h>/<R_g>$, for neutral and polyelectrolyte bottlebrush polymers. Error bars represent two standard deviations. The dot-dashed lines correspond to the reference values of the primary objects, for a smooth sphere $<R_h>/<R_g>$ is 1.29, for a rod with an aspect ratio of $A = 1550$ is 0.22, and for self-avoiding walks in θ-solvent is 0.79 [24,25].
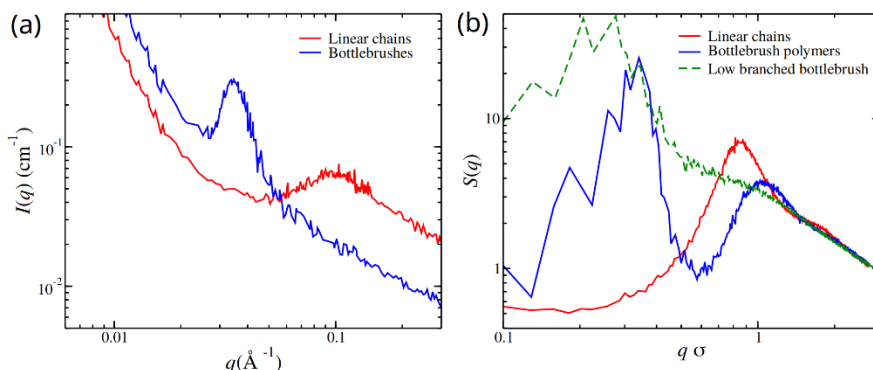
Figure 4: (a) Small angle neutron scattering profiles of salt-free solutions of linear chain polyelectrolytes (red curves) and bottlebrush polyelectrolytes (blue curves) at 4% m/m polymer concentration. (b) Structure factor of linear chain, having $M_w = 41$, and bottlebrush polyelectrolyte solutions at polymer concentration $c \approx 0.03$, having different grafting densities.

Now that we have a basic understanding of the polymer size and shape, we discuss the structure of these polymers in solution. In Fig. 4a are presented the SANS profiles of linear and bottlebrush polyelectrolytes measured at 4% m/m concentration. The linear chains have the same length as that of the bottlebrush polymer, and therefore the bottlebrush polyelectrolyte has higher molecular mass and carry more charges. The

scattering profiles exhibit a peak at q_{peak}, often called "polyelectrolyte peak". In the bottlebrush polyelectrolyte the peak appears at smaller q-values (larger distances) than in their linear counterpart, signifying that average distance between bottlebrushes is larger at the same c. Also, the peak in the case of the bottlebrush polymers is sharper, indicating that there are less fluctuations around q_{peak}. Evidently, the molecular architecture plays a crucial role in defining the position of the "polyelectrolyte peak".

To probe the structure of bottlebrush polyelectrolyte solutions, we calculate the static structure factor, $S(q)$, which describes the mean correlations in the positions of a collection of point particles distributed in space. $S(q)$ is defined as,

$$S(q) = \sum_{j=1}^{N_t} \sum_{k=1}^{N_t} \exp[-i\boldsymbol{q} \cdot (\boldsymbol{r}_j - \boldsymbol{r}_k)], \qquad (1)$$

where $i = \sqrt{-1}$, $q = |\boldsymbol{q}|$ is the wave number, r_j is the position of particle j, $< >$ denote the time average, and N_t is the total number of polymer segments defined as $N_t = N_p M_w$. The experimental observations mentioned above are supported by our model, see Fig. 4b. However, bottlebrush polyelectrolytes, based on our model, exhibit an additional peak that is absent in the experimental system. To better understand these observations, we examine the case of neutral bottlebrush polymers in solution.

Neutral polymers exhibit a peak in $S(q)$ in the low q-region, corresponding to the average inter-molecular distance (see Fig 5a). The peak occurs at $q\,\sigma \approx 0.2$ or simply $r / \sigma = 2\pi / q \approx 20$. For charged bottlebrush polymers in solution of the same polymer concentration, there are two peaks. The first peak corresponds to the average inter-molecular distance similar to the peak found in neutral bottlebrush polymers. The second peak occurs at higher q-values, $q\,\sigma \approx 1$ that corresponds to $r / \sigma \approx 6$, suggesting that this peak provides information for intra-molecular structural features of polyelectrolyte bottlebrush solutions which are absent in neutral bottlebrush polymer solutions. To confirm this observation, we calculated the form factor $P(q)$ of the bottlebrush polymers; $P(q)$ is calculated similarly to $S(q)$ except that it does not include the inter-molecular correlations. We find that the second peak is also present in $P(q)$ confirming that it is associated with intra-molecular features of the charged bottlebrush polymers. A visual comparison of typical molecular conformations of neutral and charged bottlebrush polymers points to the packing of the side chains. In neutral bottlebrush polymers, the side chains exhibit random walk mas scaling (not shown here) and they do not exhibit any spatial association. The latter is expected since the molecular interactions between them are short ranged, originating from excluded volume interactions; the attractive interactions are neutralized by the competitive interactions from the interacting solvent particles. In the case of charged bottlebrush polymers, the side chains carry charges that result in effective repulsive interactions, which force the side chains to increase their average distance from each other and stretching the backbone of the bottlebrush polymer. A secondary peak has been observed earlier by x-ray scattering measurements made on neutral highly branched bottlebrush polymer fluids [26,27], suggesting that the bottlebrush polyelectrolyte model utilized in our study may have higher grafting density than the experimental bottlebrushes used in this study. We compared the resulting $S(q)$ bottlebrush polymers having a lower number of side chains and the secondary peak disappears.

The effective repulsive interactions originating from charged polymer brushes not only influence the intra-molecular structure, as discussed above, but they also cause the bottlebrush polymers to exhibit long-range liquid-like ordering in solution. Indeed,

the majority of counter-ions are not condensed on the polymer brushes to reduce the bare polymer charge but remain solvated in close proximity to the bottlebrush often found between the side chains, see Fig 1c, resulting in a diffuse ionic cloud that "dresses" the polymer, an effect discussed in previous studies [15,16,28,29]. This diffuse ion cloud contributes to the polarizability of the polymer. Moreover, the long range electrostatic interactions are not completely screened due to the lack of salt in our systems, implying that charged bottlebrush polymers interact with each other over a longer distance scale then their neutral counterparts. The long range interactions influence on the structure can be more clearly seen in the inset of Fig. 5a. For neutral bottlebrush polymers, the inter-molecular pair-correlation function, $g(r)$ increases gradually from zero at $r / \sigma = 5$ to unity at $r / \sigma \approx 20$, which means that within this range the bottlebrush polymers start to interact with each other. For charged bottlebrush polymers, $g(r)$ increases from zero at larger distances compared to neutral bottlebrush polymers $r / \sigma = 15$ and at $r / \sigma \approx 22.5$, we find a peak in $g(r)$ similar to the one found in simple liquids. These results signify that the effective size of the polymer is increased by a factor of three due to electrostatic repulsion, which is consistent with a visual comparison between neutral and polyelectrolyte bottlebrushes in Fig. 5b. Moreover, long-range repulsive interactions lead to liquid-like packing that is absent in the analogous neutral bottlebrush polymer solutions.
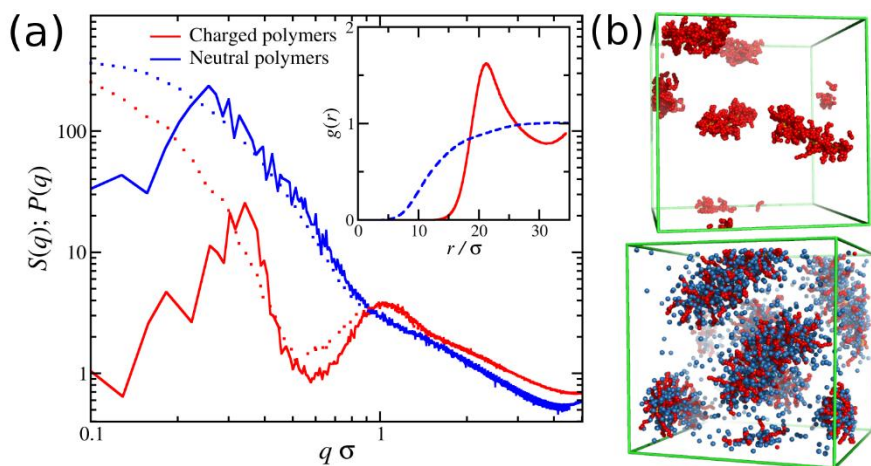
Figure 5: (a) Static structure factor $S(q)$ (continuous lines) and form factor $P(q)$ (dotted lines) of neutral and charged bottlebrush polymers in solution. Inset: radial distribution function $g(r)$ describing the inter-molecular correlations between the bottlebrush polymers in solution; the continuous and dashed lines represent polyelectrolyte and neutral bottlebrush polymers. (b) Screenshots of neutral bottlebrush polymers (top) and charged bottlebrush polymers (bottom) at the same polymer concentration; the neutral solvent is rendered invisible for visualization purposes, and the counter-ions are in blue color.

CONCLUSIONS

In summary, we investigated the structure of neutral and charged bottlebrush polymers in dilute salt-free solutions. Molecular dynamics simulations were utilized with the use of a coarse-grained bead-spring model that includes an explicit solvent. Our simulation

results are discussed in conjunction with SANS results. We find that the electrostatic interactions stretch both the side chains and the bottlebrush backbone, resulting in significant polymer swelling. Charged bottlebrush polymers exhibit an additional peak in the form and static structure factors, a feature that is absent in the neutral polymers. We show that this peak describes the intra-molecular correlations between the charged side chains. We plan to investigate this effect in future work.

ACKNOWLEDGMENTS

References

1. I. N. Haugan, M. J. Maher, A. B. Chang, T. P. Lin, R. H. Grubbs, M. A. Hillmyer, and F. S. Bates, ACS Macro Lett. 7, 525 (2018).
2. G. M. Miyake, R. A. Weitekamp, V. A. Piunova, and R. H. Grubbs, J. Am. Chem. Soc. 134, 014249 (2012).
3. W. F. M. Daniel, J. Burdyńska, M. Vatankhah-Varnoosfaderani, K. Matyjaszewski, J. Paturej, M. Rubinstein, A. V. Dobrynin, and S. S. Sheiko, Nat. Mater. 15, 183 (2016).
4. A. Chremos and J. F. Douglas, J. Chem. Phys. 149, 044904 (2018).
5. J. M. Sarapas, E. P. Chan, E. M. Rettner, and K. L. Beers, Macromolecules 51, 2359 (2018).
6. A. Chremos and J. F. Douglas, Phys. Rev. Lett. 121, 258002 (2018).
7. L. Ng, A. J. Grodzinsky, P. Patwari, J. Sandy, A. Plaas, and C. Ortiz, J. Struct. Biol.. 143, 242 (2003).
8. F. Horkay, P. J. Basser, A.-M. Hecht, and E. J. Geissler, J. Chem. Phys., 128, 135103 (2008).
9. H. Watanabe, Y. Yamada, and K. Kimata, J. Biochem. 124, 687 (1998).
10. P. J. Basser, R. Schneiderman, R. A. Bank, E. Wachtel, and A. Maroudas, Arch. Biochem. Biophys. 351, 207 (1998).
11. M. J. Stevens and K. Kremer, J. Chem. Phys. 103, 1669 (1995).
12. S. Liu and M. Muthukumar, J. Chem. Phys. 116, 9975 (2002).
13. M. Ullner and C. E. Woodward, Macromolecules 35, 1437 (2002).
14. T. S. Lo, B. Khusid, and J. Koplik, Phys. Rev. Lett. 100, 128301 (2008).
15. A. Chremos and J. F. Douglas, Soft Matter 12, 2932 (2016).
16. A. Chremos and J. F. Douglas, J. Chem. Phys. 144, 164904 (2016).
17. A. Chremos and J. F. Douglas, J. Chem. Phys. 147, 241103 (2017).
18. A. Chremos and J. F. Douglas, J. Chem. Phys. 149, 163305 (2018).
19. A. Chremos, A. Nikoubashman, and A. Z. Panagiotopoulos, J. Chem. Phys. 140, 054909 (2014).
20. M. Andreev, A. Chremos, J. J. de Pablo, and J. F. Douglas, J. Phys. Chem. B 121, 8195 (2018).
21. M. Andreev, J. J. de Pablo, A. Chremos, J. F. Douglas, J. Phys. Chem. B 122, 4029 (2018).
22. P. J. Lindner, Appl. Cryst. 33, 807 (2000).
23. J. Paturej and T. Kreer, Soft matter 13, 8534 (2017).
24. M. L. Mansfield and J. F. Douglas, Macromolecules 41, 5422 (2008).
25. M. L. Mansfield and J. F. Douglas, J. Chem. Phys. 139, 044901 (2013).
26. C. R. López-Barrón, A. H. Tsou, J. M. Younker, A. I. Norman, J. J. Schaefer, J. R. Hagadorn, and J. A. Throckmorton, Macromolecules 51, 872 (2018).
27. Z. Qian, Y. P. Koh, M. R. Pallaka, A. B. Chang, T. P. Lin, P. E. Guzmán, R. H. Grubbs, S. L. Simon, and G. B. McKenna, Macromolecules 52, 2063 (2019).
28. A. Chremos and J. F. Douglas, ACS Symp. Ser 1296, 15 (2018).
29. A. Chremos and J. Douglas, Gels 4, 20 (2018).